Hindawi
Advances in Materials Science and Engineering
Volume 2020, Article ID 4058452, 14 pages
https://doi.org/10.1155/2020/4058452

Research Article

Tensile Fracture Behavior of Corroded Pipeline: Part 1—Experimental Characterization

Yuchao Yang[1], **Feng Liu**[1] and **Feng Xi**[2]

[1]*Shandong University of Science and Technology, Shandong Provincial Key Laboratory of Civil Engineering Disaster Prevention and Mitigation, Qingdao 266590, China*
[2]*School of Civil Engineering, Shandong Jianzhu University, Jinan 250101, China*

Correspondence should be addressed to Feng Liu; feng.liu@sdust.edu.cn

Received 15 September 2019; Revised 12 January 2020; Accepted 17 January 2020; Published 18 February 2020

Academic Editor: Pasquale Gallo

The understanding of the axial tensile behavior of environmentally corroded pipelines is of great significance for the design, maintenance, and evaluation of such structures. This article presents some experimental data recorded from 210 tensile tests on pipe, which were corroded from grade of 10% to 70% by electrochemical accelerated corrosion method. The fracture modes show that, for the uncorroded pipe, the fracture frequently occurs in the middle of the specimen and then propagates perpendicular to the loading direction. However, for the corroded pipe, the crack's position, evolution angle, and path have strong randomness. The comparative analysis based on the macroscopic stress-strain relationship shows that the rapid decrease of the yield stress, ultimate strength, and strain at the fracture for corroded pipe are correlated with the fracture patterns; i.e., the fracture patterns of pipe are changed from uniform to scattered with the continuous increase of the corrosion rate. The reduction factor based on experimental data is recommended for the consideration of the corrosion effect on the tensile strength of the steel pipe. Discussion on the tensile capacity during the service time is also presented.

1. Introduction

Pipelines have been widely used in various engineering, e.g., nuclear plant, petrochemical project, or marine platforms. Since its particular importance, it is always referred to as the artery of the national economy. Many scholars have conducted numerous studies on the mechanical properties of uncorroded pipelines [1–4]. Unfortunately, due to their aging and features of the materials, pipelines are incredibly vulnerable to external environmental erosion which may result in defects in generation and then reduce their reliability together with a series of catastrophic chain reactions. It is generally accepted that the corrosion has been becoming an urgent threat during the service life of pipelines [5–7].

Previous studies have shown that the mechanical performance of corroded pipelines is mainly attributed to two levels. The first one is the change of metallographic structure of the pipeline material, and the other one is the degradation of its section characteristics. For the first level, although a lot of experimental research has been carried out, there seem to be contradictory conclusions. For example, Li et al. [8] and Almusallam [9] found that the corrosion only reduced the cross-sectional area, and the metallographic structure did not change. However, Imperatore et al. [10] believed that when the metal is eroded, the crystal lattice of the material will be alerted simultaneously and then degrade its performance.

For the second level, the current research mainly focuses on the burst pressure of corroded pipes. For example, based on the experimental data and theoretical analysis, some guidelines or recommendations have been proposed for evaluating the critical pressure or residual strength of corroded pipelines (e.g., ASME B31G [11], modified ASME B31G [12], and DNV RP101 [13]). At another area of this level, work has been concentrated on the evaluation of the bending behavior of corroded pipes; e.g., Bai and Hauch [14] explored it by assuming the pipeline has constant depth rust pitting, and Han et al. [15] and Kim et al. [16] investigated it

using the net section failure method. Besides, Kim et al. [17] studied the effect of stress concentration caused by corrosion on the fracture behavior of pipelines and proposed a prediction formula for the service life of pipelines considering stress concentration, and Mokhtari and Melchers [18] proposed a new finite element model to predict the residual strength of corroded pipelines.

Despite extensive work reported, there is a surprising lack of literature specially relating to the tensile behavior of the corroded pipeline. In fact, there exists a potential risk that the pipeline would be subject to axial action during service. These axial effects would come from ground motions, landslides, or waves caused by submarine circulation. During these loading cases, the supports at both ends of the span will be displaced relatively, which will cause the pipeline within the span to fail due to approximate tension or compression. In this field, Ye et al. [19] studied the performance of a corroded pipeline under the combined action of tensile and external pressure through a numerical simulation method for models with uniform symmetrical defects in the axial direction. It was found that the critical external pressure for pipeline failure decreases with the increase of axial stretching. In addition, Zhu and Leis [20] studied the influence of yield-to-ultimate strength on the performance of corroded pipelines and proposed a strength degradation model, and Rajapipour and Melchers [21] investigated the pipeline with pitting on the external surface under axial compression and internal pressure by the finite element analysis and found that the critical load of the pipe is extremely sensitive to the shape and depth of the rust pit.

The above research on the corroded pipeline under axial action mainly focused on compression loading, primarily relied on theoretical research methods, and still lacks experimental data support. Therefore, there is still no comprehensive and systematic understanding of the influencing factors and mechanical mechanisms of the tensile performance of corroded pipelines. This need motivated the current study.

The primary objective of this paper is to provide experimental evidence and develop mechanism understanding for tensile fracture characteristics of the corroded pipe. In the first part, the seamless round steel pipe with outer diameter $D = 25$ mm and wall thickness $H = 1$ mm is corroded by the electrochemical accelerated corrosion method, and the key factors affecting its performance were identified by comparing the fracture modes and macroscopic stress-strain curves. Based on this, the second part is devoted to the establishment of the pipe wall thickness distribution field following the actual distribution and maps it into the finite element model to carry out parameter analysis to understand the failure mechanism of the corroded pipe under axial tension.

This paper is organized as follows: Test pipeline specimen and its material properties are described in Section 2. The corrosion process and its characterization are illustrated in Section 3. Test results are shown in Section 4 to demonstrate the influence of corrosion rate on the tensile performance. Discussion on the results and engineering implications are presented in Section 5, which is followed by conclusions.

2. Test Pipe and Material Properties

Studies by Kucheryavyi and Mil'kov [22] and Kou [23] showed that the diameter of commonly used oil and gas pipelines in actual engineering is about 150 mm to 2000 mm, and the diameter-thickness ratio is about 10 to 170 considering the transportation capacity, the distance between stations, and internal pressure. Due to the capabilities of experimental equipment and operability of artificial corrosion, it's challenging work to directly conduct the test on an original pipe; therefore, the scale model is adopted in the present test to investigate its mechanical performance.

Generally, static tests for scale model need to meet similarity requirements in geometry, material, load, and boundary conditions. In the present paper, the test specimen is selected and has the same material as the prototype pipe, but the geometry dimension is 1/10 of the prototype. According to similitude theory, other parameters can be obtained by these two key factors, which are summarized in Table 1.

In the present study, a seamless round steel pipe with an outside diameter of $D = 25$ mm and a wall thickness of $H = 1$ mm was selected as test specimen. According to Chinese code about the metallic material tensile testing method (GB/T 228.1-2010) [24], the tensile test was conducted by directly cutting a standard length of the pipe from the test specimen. As shown in Figure 1, MTS test machine is used to perform the tensile test. The specimen has a total length of 210 mm, with an intermediate gauge length of 50 mm. Two hemispherical shaped high-strength steel chock plugs with diameter of 23 mm were inserted at both ends of the pipe to prevent the collapse of the specimen in the clamped section during the stretching. The loading scheme was displacement controlled, and the moving speed of the chuck of the testing machine was set to 1.8 mm/min. The strain rate was approximately $2.5 \times 10^{-4}\ \mathrm{s}^{-1}$, which can be considered as a quasi-static tensile test, and the strain-rate effect could be safely neglected. To ensure the test data are repeatable, three specimens were stretched following the same loading strategy.

As shown in Figure 2, the fracture occurred approximately in the middle of the gauge length, and the shape of the breach is relatively neat, which indicates that the stress distribution on the same cross-section was nearly uniform during the stretching process.

The present paper aims to study the macroscopic tensile performance of the pipeline. Therefore, the nominal stress calculated by $\sigma = F/A$ was used to construct the stress-strain curve, where F is tensile force recorded by the testing machine and A is cross-sectional area before the pipe was stretched. This area was calculated by $A = m/(\rho L)$, in which m, ρ, and L are the mass, density, and length before pulling the pipe, respectively. ρ is set as $7800\ \mathrm{kg/m^3}$ in the present study. Figure 3 shows the recorded stress-strain curve of the uncorroded specimen; the elastic modulus, yield stress, and ultimate strength were identified as 208.5 GPa, 304.5 MPa, and 439.3 MPa. Furthermore, the strain at the fracture was approximately 0.235, which can be judged as good plasticity.

Table 1: Similitude scale factors for present test specimen.

	Parameter	Relationship	Model/prototype
Geometry	Length (L), diameter (D), thickness (t)	S_L	1/10
	Elastic modulus (E)	S_E	1
Material	Stress (σ)	$S_\sigma = S_E$	1
	Strain (ε)	S_σ/S_E	1
Force	Axial force (F)	$S_\sigma \cdot S_L^2$	1/100
	Boundary conditions	The same as the prototype	

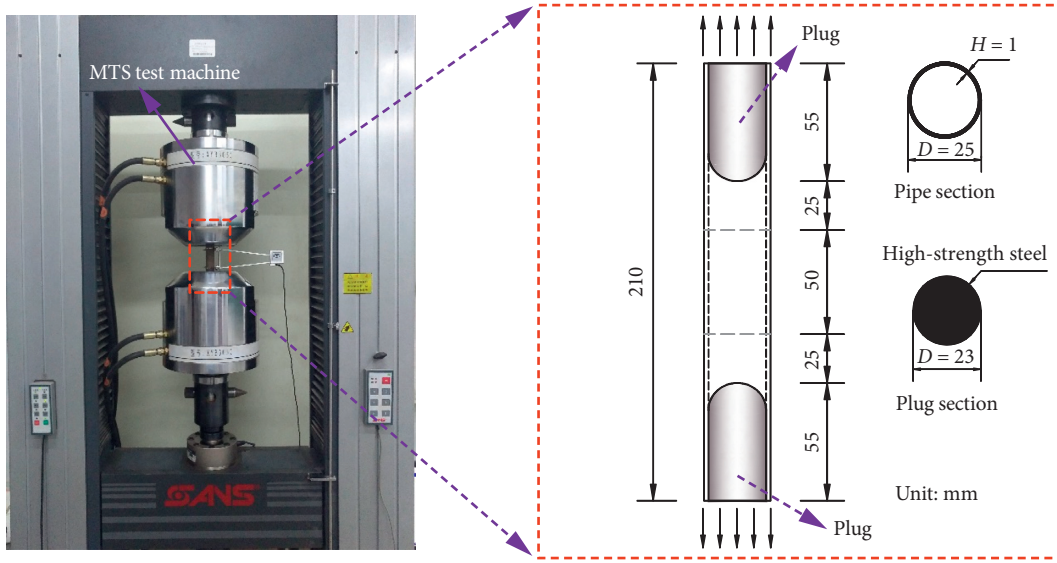

Figure 1: Tensile test setup and specimen size.

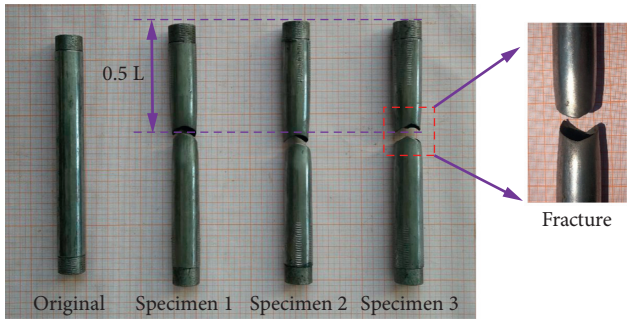

Figure 2: Fracture patterns with an uncorroded pipe under uniaxial stretch.

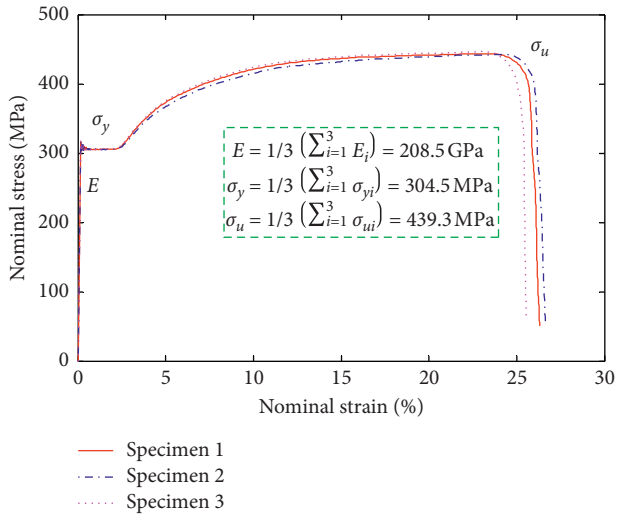

Figure 3: Recorded nominal stress-strain curve of uncorroded pipe.

3. Pipe Corrosion

Wang et al. [25] recommended dividing the corrosion into four types: general corrosion, pitting corrosion, grooving corrosion, and edge corrosion. Due to space limitations, the present paper only reports the results of the general corrosion type.

3.1. Fundamental Theory. Four options were frequently used to obtain corroded pipe specimens, i.e., (1) removing the corroded components from the actual engineering structures [26], (2) accelerating the corrosion in an artificial environment [27], (3) expediting the corrosion using electrochemical techniques in a laboratory [28], and (4) using a mechanical process to simulate the corrosion [29]. Among them, laboratory electrochemical accelerated corrosion is a relatively simple and efficient method. Du et al.'s study [28] showed that the different ways might lead to variable surface

characteristics, but the degradation trend on the mechanical properties was the same. Therefore, from the perspective of efficiency, availability, and the ability to reproduce the same actual corrosive events, the specimens used in this study were all corroded using the electrochemical technique. This method is widely used in the research of steel bars [28] and steel plates [30]. Besides, according to the location and cause of the corrosion, pipeline corrosion is generally divided into two categories: inner wall and outer wall corrosion. The former is mainly caused by the fluid transported by the pipeline, and the latter is primarily attributed to the natural environment in which the pipe is located. This paper only examines the corrosion of the outer wall caused by natural environment invasion.

The basic rule abided by in electrochemically accelerated metal corrosion is Faraday's law [31] which can be expressed as

$$\Delta m = \frac{M \cdot I \cdot t}{Z \cdot F}, \tag{1}$$

where Δm is the mass loss, M is the molar mass, I is the current intensity, t is the time of power-on, Z is the absolute value of total number of positive or negative valences in the compound, and F is the Faraday constant.

The current intensity I at the surface of the steel pipe can be obtained from its current density; i.e.,

$$I = i \cdot \pi \cdot D \cdot L_c, \tag{2}$$

where i is the surface current density when the pipe is being corroded and D and L_c are outside diameter and length of the corroded section of the pipe, respectively.

Typically, the corrosion rate, η, of the pipe can be evaluated by mass reduction by

$$\eta = \frac{\Delta m}{m^I} \times 100\%, \tag{3}$$

where m^I and Δm are the original and reduced mass of the corroded segment of the pipeline, respectively.

Let r_1 and r_2 denote the outside and inside radius and ρ represent the density of the pipe; the mass of corroded segment of the pipe can be expressed as

$$m^I = \pi \cdot \left(r_1^2 - r_2^2\right) \cdot \rho \cdot L_c. \tag{4}$$

According to equations (3), (4), and considering equation (1), period t, for the given target corrosion rate η, can be predicted by

$$t = \frac{\eta F \left(r_1^2 - r_2^2\right)\rho}{M i r_1}. \tag{5}$$

Based on the principle discussed above, the electrochemical setup shown in Figure 4 was adopted for present work. After the specimen was numbered, weighed, and recorded, two ends of the specimen were bound with scotch tape on the outside surface, and a plug was inserted into the inside surface to prevent the liquid solution from entering and destroying the sample. Then, one end of the pipe was connected to the copper clamp with an electric wire, and they were put into a bracket composed of a bamboo stick

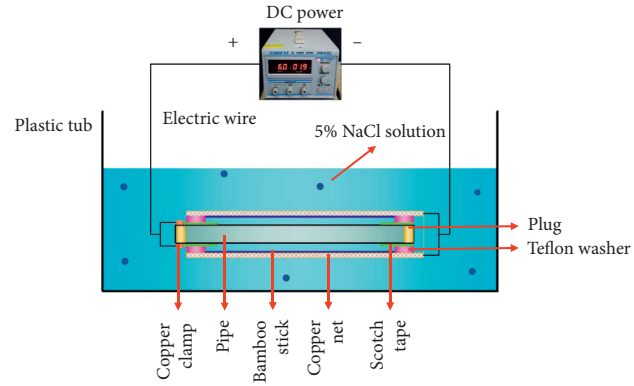

Figure 4: Schematic diagram of electrochemical corroding process.

with a Teflon gasket to support the copper net and prevent the copper net and the steel pipe from directly contacting each other (the copper net was made of pure copper). Finally, all of the components were placed in the copper net with the wire, and these were placed in a plastic tub. The copper clamp wire and the copper net wire leads were connected to the positive and negative poles of a DC power supply, respectively. During the whole process, all the specimens were combined in a parallel way.

3.2. Corrosion Process and Characterization. Figure 5 shows the implementation of the electrochemical corrosion process, which primarily included three steps. The first one was preparation. As shown in Figure 6, the length of the pipe was measured with a steel ruler (up to 0.5 mm), and the domain of interest was marked. Then, the thickness and outside diameter along the length of the pipe were measured in two orthogonal directions using an electronic vernier caliper (up to 0.01 mm). These measurements were recorded as $H_1^1, H_1^2, \ldots, H_i^1, H_i^2, \ldots, H_n^1, H_n^2$ and $D_1^1, D_1^2, \ldots, D_i^1, D_i^2, \ldots, D_n^1, D_n^2$, and the average values of the thicknesses and the diameters were calculated by

$$H = \frac{1}{2n}\sum_{i=1}^{n}\left(H_i^1 + H_i^2\right),$$
$$D = \frac{1}{2n}\sum_{i=1}^{n}\left(D_i^1 + D_i^2\right). \tag{6}$$

The second step was the actual corroding of the specimen. An appropriate amount of 5% NaCl solution was added to the plastic tub to ensure that the liquid level was higher than the surface of the copper net. Then, the DC power was connected, and the current was adjusted to the appropriate amplitude to start the corrosion process. Tamer [31] conducted electrochemical corrosion tests under similar conditions with current densities of 100–500 μA/cm^2. He found that the current density had a dominant effect on the period but was less sensitive to the corrosion feature. Therefore, the current density in this study was set to approximately 500 μA/cm^2, and then the corrosion rate of the pipeline was only dominated by the charging period.

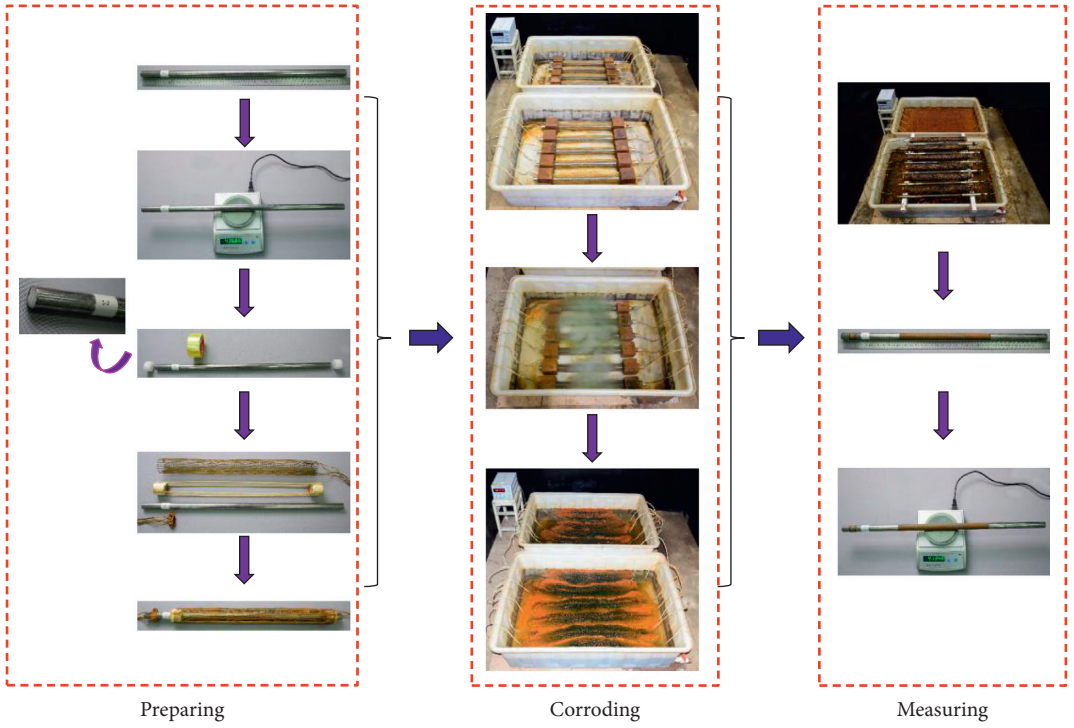

Figure 5: Process of electrochemical corroding process.

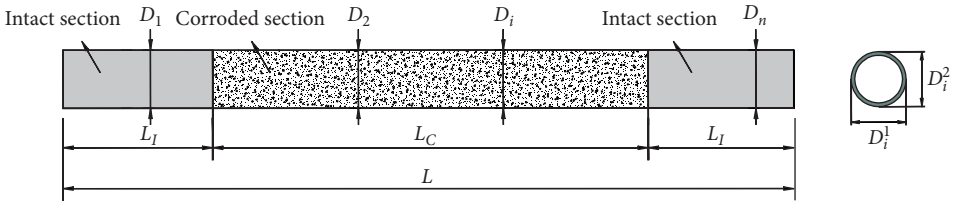

Figure 6: Demonstration of section categorization and measurement.

The third step was the measurement and characterization of the specimen. When the time predicted using equation (5) passed, the specimen was removed from the tub and immersed in a 12% hydrochloric acid solution to neutralize the remaining alkali liquid. The specimen was then placed in a drying cabinet for four hours after it was rinsed with water [28]. Finally, the weight of sample was measured and recorded using an electrical balance.

Practically, there are two ways to evaluate the corrosion rate of metal [29]. One is to calculate the mass corrosion rate or the average section corrosion rate by comparing the specimen before and after corrosion. The other method is to describe the corrosion depth per unit area using a scanning device. As the aim of this study was to investigate the macroscopic mechanical performance of corroded pipes under uniaxial tension, the general mass corrosion rate, η, was used to evaluate the corrosion rate, which can be expressed as

$$\eta = \frac{m^I - m^C}{m^I} \times 100\%, \tag{7}$$

where m^I, m^C are initial and after-corrosion weights of the domain of interest section of the specimen, respectively. As discussed in the previous section, m^I, m^C can be, respectively, calculated as

$$\begin{aligned} m^I &= m - \pi \cdot H(D-H) \cdot (L - L_C) \cdot \rho, \\ m^c &= m^* - \pi \cdot H(D-H) \cdot (L - L_C) \cdot \rho, \end{aligned} \tag{8}$$

where m and m^* are the mass of the whole specimen before and after the corrosion process, respectively.

Thus, for the selected pipe in the present study, when the current density was set to 500 μA/cm^2, the period time was approximately 430 hours for a corrosion rate of 30%. The test verification showed that the error between the theoretical predication found using equation (5) and the actual measurement was within 10%, which shows that the corrosion rate could be approximately estimated according to equation (5).

The present test corroded 210 specimens according to the above procedure and got seven grades of corrosion rates (about 10% to 70%). Table 2 shows detailed information about the selected specimen. This information includes mass, length, outside diameter, corrosion rate, and other factors. The test pieces were labeled 1-1 to 7–15. The first and

Table 2: Detailed information on the selected corroded specimen.

No.	L (mm)	D (mm)	M (g)	L_c (mm)	D_c (mm)	m^* (g)	m^I (g)	m^c (g)	η (%)	H_c (mm)	F (kN)	${\sigma_y}^C$ (MPa)	${\sigma_u}^C$ (MPa)
1-1	759.4	25.03	448.33	334.5	24.83	427.69	197.48	176.84	10.45	0.91	29.572	301.18	430.17
1–4	759.4	24.98	448.33	333.5	24.71	420.90	196.89	169.46	13.93	0.86	27.115	275.49	423.18
1–6	758.6	25.01	447.85	333.7	24.84	430.22	197.00	179.37	8.95	0.92	29.752	303.62	430.35
1–7	759.8	25.00	448.56	333.8	24.81	429.60	197.06	178.10	9.62	0.90	28.943	300.96	425.86
1–11	758.7	24.96	447.91	336.1	24.78	429.52	198.42	180.03	9.27	0.89	28.909	302.27	432.79
1–13	761.5	25.04	449.57	336.9	24.76	420.95	198.90	170.28	14.39	0.88	28.439	302.83	430.78
2-2	759.8	24.99	448.56	333.2	24.53	401.72	196.71	149.87	23.81	0.77	22.917	271.59	401.25
2–6	760.5	25.02	448.97	335.1	24.63	409.34	197.83	158.20	20.03	0.82	25.369	287.54	416.07
2–7	758.5	24.99	447.79	334.5	24.65	412.93	197.48	162.62	17.65	0.82	26.036	284.95	421.65
2–8	758.9	24.97	448.03	335.1	24.67	417.07	197.83	166.87	15.65	0.84	26.290	280.25	420.48
2–11	759.6	24.99	448.44	333.4	24.55	403.94	196.83	152.33	22.61	0.78	24.266	280.78	419.21
2–13	756.4	25.03	446.55	333.2	24.60	403.29	196.71	153.45	21.99	0.80	23.990	276.14	401.08
3–1	758.7	24.98	447.91	334.3	24.36	384.64	197.36	134.09	32.06	0.68	19.484	269.27	385.17
3-2	761.1	25.03	449.33	334.0	24.45	391.30	197.18	139.15	29.43	0.73	22.802	294.16	421.97
3–5	760.2	25.03	448.80	333.9	24.55	400.29	197.12	148.61	24.61	0.78	24.524	291.40	423.67
3–7	759.9	24.99	448.62	336.3	24.46	393.78	198.54	143.70	27.62	0.73	22.548	278.41	414.33
3–9	760.1	25.03	448.74	333.2	24.35	381.19	196.71	129.16	34.34	0.68	21.219	290.53	422.67
3–15	759.6	24.95	448.44	331.9	24.37	388.38	195.94	135.88	30.65	0.69	20.788	278.81	407.86
4–1	759.7	25.03	448.50	333.5	24.32	377.34	196.89	125.73	36.14	0.66	18.667	271.43	380.53
4-5	760.4	25.00	448.92	336.1	24.24	371.48	198.42	120.98	39.03	0.62	13.350	179.12	290.18
4–6	761.2	24.96	449.39	335.8	24.13	363.57	198.25	112.43	43.29	0.57	14.390	240.39	344.05
4–9	759.7	25.02	448.50	335.4	24.21	367.24	198.01	116.75	41.04	0.61	15.096	229.29	336.49
4–12	760.6	24.98	449.03	333.2	24.19	368.60	196.71	116.28	40.89	0.60	18.936	301.65	429.36
4–15	760.8	24.98	449.15	334.7	24.19	367.98	197.60	116.43	41.08	0.60	16.781	238.86	380.49
5–1	760.4	24.98	448.92	333.1	24.07	356.77	196.65	104.50	46.86	0.54	13.500	241.26	341.29
5–3	761.2	25.00	449.39	334.7	23.93	341.95	197.60	90.16	54.37	0.47	9.955	181.39	290.43
5-6	758.9	24.98	448.03	333.6	23.95	344.02	196.95	92.94	52.81	0.48	10.582	215.61	302.10
5–9	760.0	25.00	448.68	334.6	23.98	345.74	197.54	94.60	52.11	0.49	12.409	233.26	343.19
5–12	760.7	25.01	449.09	335.1	24.03	350.21	197.83	98.95	49.98	0.52	16.192	296.91	425.61
5–15	761.1	25.04	449.33	334.3	24.00	346.98	197.36	95.01	51.86	0.50	11.995	235.05	324.97
6–1	760.3	25.01	448.86	334.1	23.84	332.45	197.24	80.83	59.02	0.42	8.829	202.62	285.74
6–2	759.2	25.04	448.21	333.0	23.74	321.33	196.59	69.71	64.54	0.37	10.571	252.53	389.16
6–8	761.2	25.03	449.39	332.4	23.78	326.76	196.24	73.61	62.49	0.39	8.914	195.32	311.06
6–9	761.0	25.00	449.27	334.2	23.82	330.52	197.30	78.55	60.19	0.41	7.949	189.19	263.64
6–12	757.0	25.01	446.91	335.7	23.85	330.30	198.19	81.58	58.84	0.43	9.015	176.18	288.26
6–15	757.2	24.96	447.03	332.7	23.72	321.16	196.42	70.55	64.08	0.36	6.947	173.72	262.95
7–2	758.9	25.02	448.03	335.3	23.49	297.01	197.95	46.93	76.29	0.24	2.620	103.48	146.44
7–3	760.5	25.01	448.97	334.2	23.58	306.78	197.30	55.11	72.07	0.29	4.245	145.25	200.07
7-7	760.5	25.01	448.97	331.7	23.72	321.30	195.82	68.15	65.20	0.36	6.240	171.07	236.19
7-8	760.1	25.02	448.74	333.6	23.65	313.42	196.95	61.63	68.71	0.32	4.768	128.43	200.21
7–11	761.1	24.99	449.33	332.6	23.62	312.25	196.36	59.28	69.81	0.31	4.295	141.05	189.20
7–15	757.5	24.97	447.20	333.7	23.59	307.29	197.00	57.09	71.02	0.30	4.683	140.25	216.95

L is the total length of pipe; L_c is the length of corroded section of pipe; M is the total mass of pipe before it was corroded; D_c is the average outer diameter of corroded section of pipe; H_c is the average thickness of corroded pipe; F is the maximum tension force recorded during the test; ${\sigma_y}^C$ and ${\sigma_u}^C$ are yield and ultimate strength of the corroded pipe.

second number represent the number of the batch and the sequence in the same batch, respectively. It can be observed that even if the external conditions were the same for the same batch, the corrosion rate of each pipeline was always different due to the dispersion of the material on the specimen and differences in the electric field distribution around them. For example, two pipes numbered 3–7 and 3–9 are the same batch of samples with a target corrosion rate of 30%, but the corrosion rates are 27.62% and 34.34%, respectively. This phenomenon suggests that actual pipelines serving in complex natural environments may have more significant differences in corrosion rate and rust characteristics.

3.3. Surface Topology of Corroded Pipe. To compare the features of the outside surfaces of the corroded specimen, Figure 7 shows scanning electron microscopic (SEM) images of the outer surface of the original pipe and pipes with corrosion rate of 9.62%, 31.57%, and 68.71%, respectively. At 150-time magnification, the original pipe surface (Figure 7(a)) showed no significant color difference and surface unevenness except for a few subtle scratches. For the pipe of a corrosion rate of 9.62% (Figure 7(b)), sporadically scattered pitting appears on the outer surface of the pipe, and the rest remains almost the same as the original surface.

However, the outer surface of the pipe gradually exhibits distinct and irregular color differences and thickness

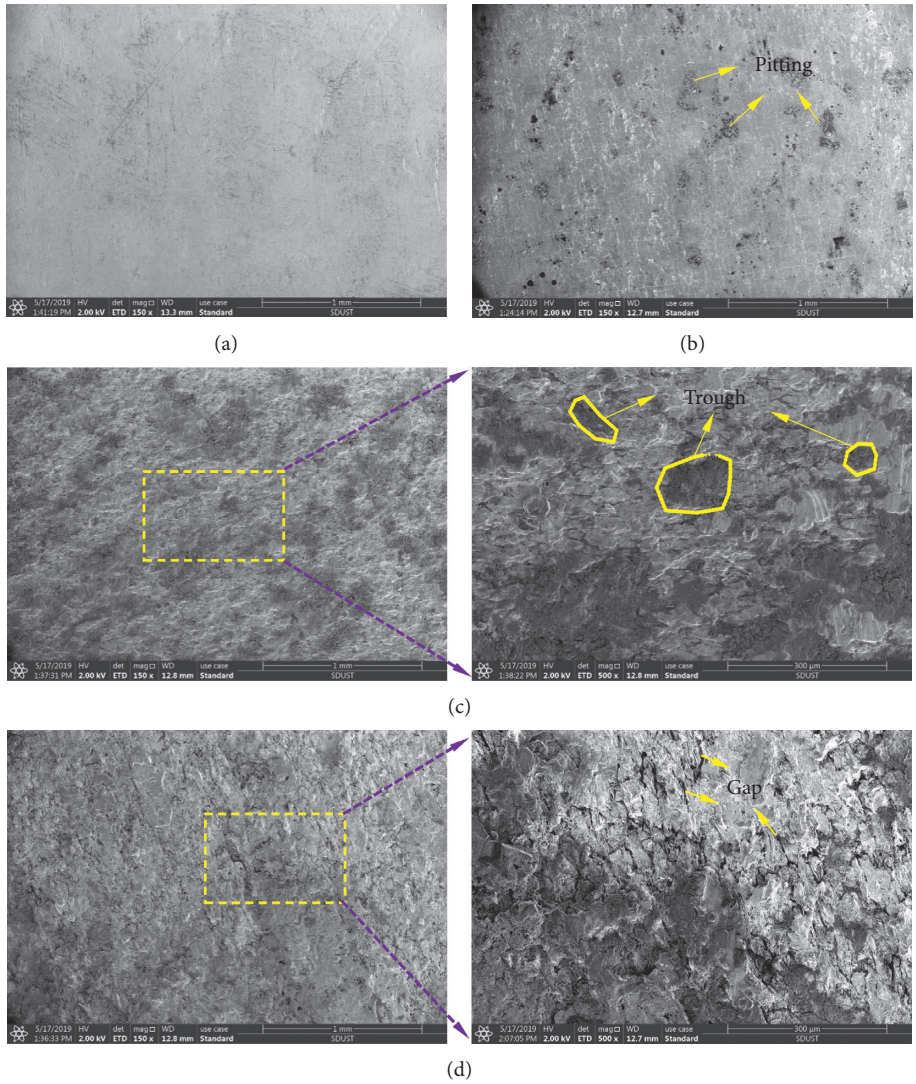

Figure 7: SEM images of the outside surface of pipe specimen: (a) uncorroded pipe; (b) pipe with corrosion rate of 9.62%; (c) pipe with corrosion rate of 31.57% (left: 150 times; right: 500 times); (d) pipe with corrosion rate of 68.71% (left: 150 times; right: 500 times).

distribution as the corrosion rate increases. For rate of 31.57% (Figure 7(c)), the surface is covered with hilly rust pitting with irregular shapes and positions, and for rate of 68.71% (Figure 7(d)), the surface is densely distributed with "grooved" cracks, and thereby the material is divided into a plurality of regions of different shapes and thicknesses. This phenomenon is not apparent in the pipeline with low corrosion rate, indicating that the uneven distribution of the wall thickness of the pipe may be aggravated with the increase of the corrosion rate.

4. Tensile Fracture Behavior of Corroded Pipe

4.1. Fracture Modes. To obtain the tensile fracture behavior of corroded pipe, a series of stretch tests were conducted, and the test setup and loading strategy were exactly the same as those used for the intact pipe as illustrated in Section 2.

Figures 8 and 9 show photographs of fractures of pipes with different corrosion rates. It is easy to find that when the corrosion rate is lower (Figure 8), there exists only one main crack. Besides, instead of being limited to the middle section like the uncorroded pipe, its position is more dispersed. The evolution path of these cracks is horizontal (Figure 8(d)) or oblique (Figure 8(b)); some behave like spirals (Figure 8(c)).

For the pipelines with corrosion rate around 45%–70% (Figure 9), the crack development is significantly different from the pipelines with previously lower corrosion rate. Not only is the location of the fracture more random, but also the generation of adjacent secondary fractures during the production and expansion of the primary fracture (Figures 9(b)–9(d)).

To understand the randomness of crack initiation position and evolution path, as shown in Figure 10, we constructed a Cartesian coordinate system with the center of the horizontal projection of the pipeline as the origin, and the longitudinal and horizontal axes, respectively, point to the stretching and radial direction. If the distances for farther and closer end of the crack (points A and B in Figure 10)

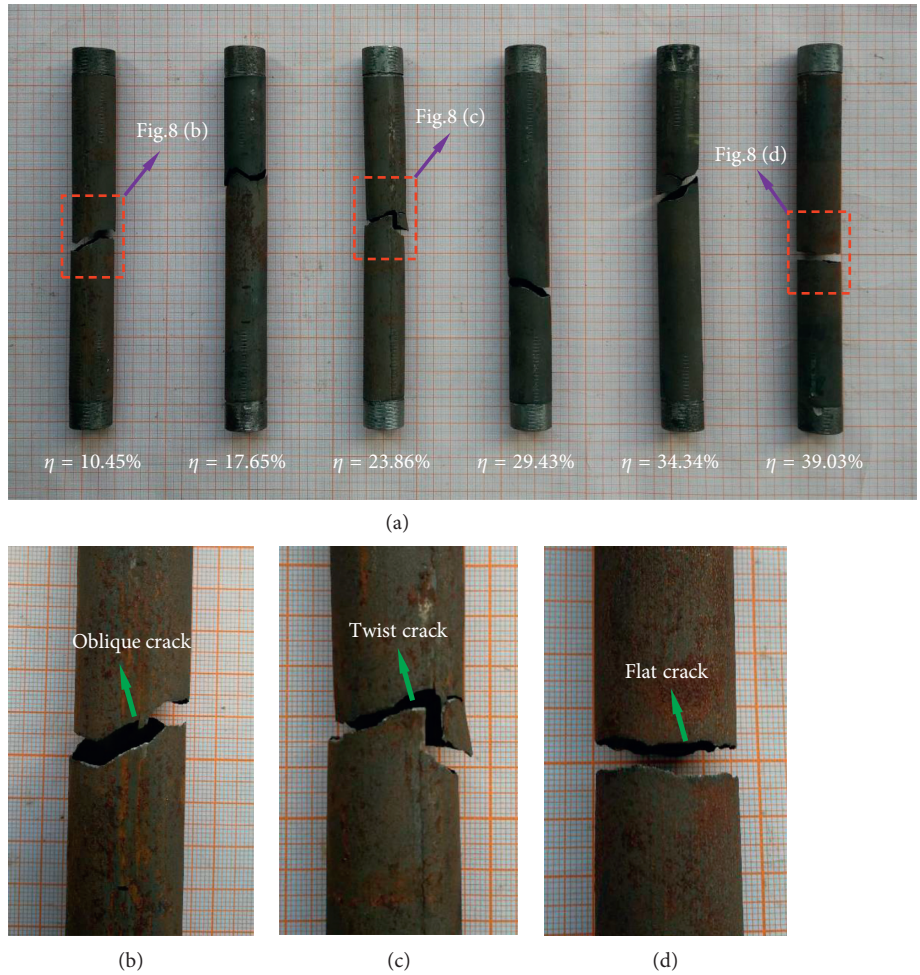

Figure 8: Fracture patterns of corroded pipe with lower corrosion rates.

relative to the x-axis are L_T and L_B, and the angle between the line AB and y-axis is θ, then the position and the angle of crack can be characterized by the following dimensionless quantities:

$$\mu_p = \frac{\left|L_T + L_B\right|}{L_M}, \tag{9a}$$

$$\mu_\theta = \frac{2\tan^{-1}\left[2R/\left|L_T - L_B\right|\right]}{\pi}, \tag{9b}$$

where L_M is the distance between two clamping ends in the test machine; for the present test, it is 120 mm. Normally, the μ_p, and μ_θ should fall into the range of $\mu_p \in [0, 1]$ and $\mu_\theta \in (0, 1]$. For the uncorroded pipe, which was tested in the present paper, the μ_p and μ_θ obey the rule of $\mu_\theta \approx 1$, $\mu_p \in [0, (1/4)]$.

To investigate the crack distribution characteristics of corroded pipes, Figure 11 shows the distribution of μ_p and μ_θ for all 210 pipes. It can be seen that the distribution of μ_p is extremely discrete, and it is difficult to summarize its regularity. Since the uniaxial tensile fracture behavior of the pipeline mainly reflects the axial distribution characteristics of the sections, the randomness of the failure location reveals the unevenness of the wall thickness along the tensile direction. On the other hand, the distribution of μ_θ is clearly expressed in two different regions: most of the values are in the range of [0.4, 1], and very few are in the range of [0.0, 0.4]. It is noted that the $\mu_\theta = 0.0$, $\mu_\theta = 0.5$, and $\mu_\theta = 1.0$ represent the evolution angles 0°, 45°, and 90°, respectively, which are the fracture modes corresponding to the typical uncorroded pipe under the hoop expanding, the biaxial stretching, and the uniaxial tension in the longitudinal direction. Therefore, the random distribution of the μ_θ indicates that the corroded pipe is jointly controlled by a uniaxial stress state or a biaxial stress state during the axial stretching. Since the hoop stress of the corroded pipe is only introduced via Poisson effect, its amplitude is usually small. Therefore, the biaxial stress state in the corroded pipe should reflect the nonuniformity of the cross-section in the circumferential distribution of the pipe.

4.2. Stress-Strain Curves of Corroded Pipe. Calculation of the stress-strain curve for the corroded specimen is a challenging task as the area of the specimen along its length is random and nonuniform. For comparison with the results of the intact specimen and for understanding the mechanical

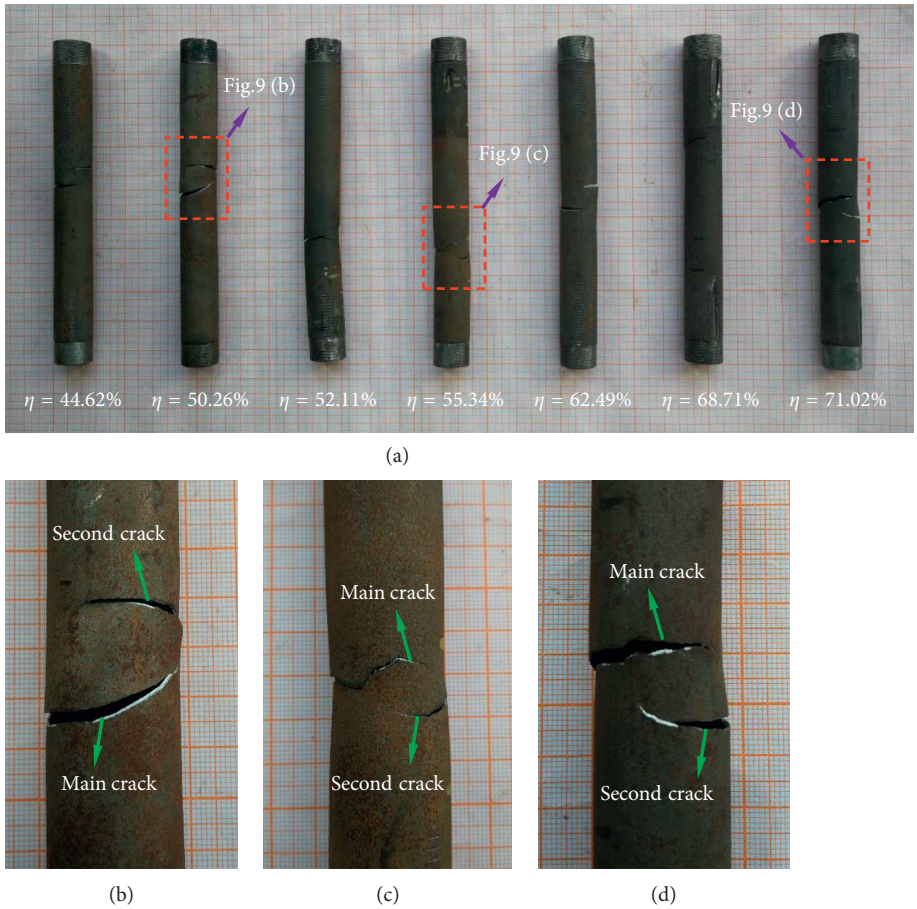

Figure 9: Fracture patterns of corroded pipe with higher corrosion rates.

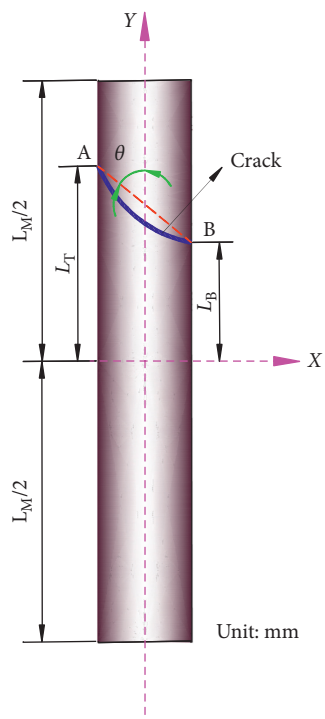

Figure 10: Schematic demonstration of crack location and evolution path.

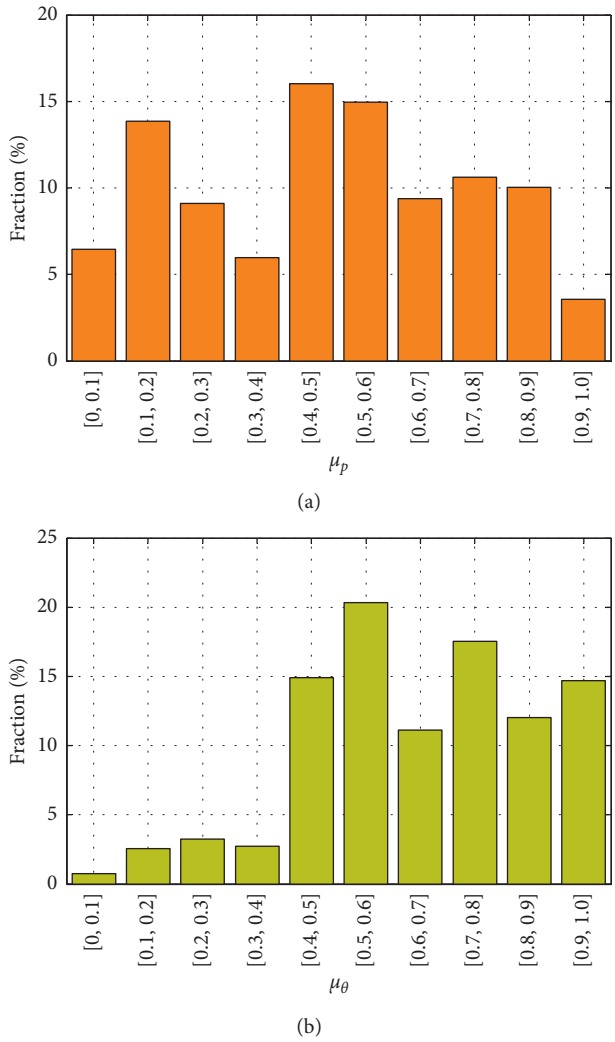

Figure 11: Statistical information of corroded pipe's crack: (a) location; (b) evolution angle.

properties from a macroscopic perspective, equation (10) was used in the present study to achieve the stress from the recorded reaction force, F,

$$\sigma^C = \frac{F}{A^C}, \tag{10}$$

where $A^C = m^C/(\rho L_C)$ is a nominal section area before the corroded pipe is stretched. It should be noted that the result of equation (10) is the stress of the material in unit area so that it can be directly compared to the value of the uncorroded specimen. Thus, the variation on its value should not be thought of as a decrease in the area, but be attributed to the heterogeneity of the surface due to the corrosion.

Figure 12 draws the stress-strain curves of the corroded specimen with corrosion rates in the range of 8.95%–71.02%, respectively. Generally, the yield strength ${\sigma_y}^C$, ultimate strength ${\sigma_u}^C$, and strain at fracture $\varepsilon_{\mathrm{pl}}^C$ decrease as the corrosion rate increases. However, this phenomenon does not strictly obey the monotonic decrease trend. For example, the strength of a specimen with a rate $\eta = 39.03\%$ is significantly lower than the value of a specimen with $\eta = 40.89\%$. This phenomenon implies that, in addition to the corrosion rate, the nonuniformity of thickness distribution introduced from the corrosion may be another crucial factor that affects their mechanical properties. Besides, the elastic modulus does not change significantly during the entire corrosion period, which reveals that the corrosion process may not influence the metallographic structure of a specimen.

5. Discussion on the Results and Engineering Implications

The trend of mechanical properties of corroded pipelines is an important issue of engineering design and evaluation. Therefore, we define dimensionless parameters as shown in equation (11), to characterize the changes in yield strength and tensile strength, respectively.

$$\lambda_y = \frac{{\sigma_y}^C}{\sigma_y}, \tag{11a}$$

$$\lambda_u = \frac{{\sigma_u}^C}{\sigma_u}. \tag{11b}$$

The statistical data are presented in Figure 13, and the regression formulas are shown in Equation (12). They show that although there is a discrete type, the pipe's strength shows an evident decreasing trend with the increase of the corrosion rate. For example, when the pipe corrosion rate reaches 10% and 50%, the yield strength and ultimate strength are only 97%, 76% and 97%, 75% of the uncorroded pipelines. This trend is consistent with the findings of corroded steel bars or plates, e.g., Maslehuddin et al. [32], Ou et al. [33], Gu et al. [34], and Wang et al. [35]. In addition, more detailed observations show that the dispersion of the strength index increases remarkably with the increase of the corrosion rate, which may be closely related to the trend that the nonuniformity of the pipe wall thickness increases with the increase of the corrosion rate.

$$\lambda_y = 1 - 0.25\eta + 0.15\eta^2 - 1.2\eta^3, \tag{12a}$$

$$\lambda_u = 1 - 0.19\eta - 0.09\eta^2 - 1.0\eta^3. \tag{12b}$$

The above discussion focuses on changes in the macroscopic properties of pipelines caused by environmental erosion, while the carrying capacity may be more concerned in the engineering field. According to Equation (12), the degradation factor for the tensile capacity for the corroded pipelines can be expressed as

$$\begin{aligned}\lambda_F &= \frac{{F_u}^C}{F_u} \\ &= \frac{\left({\sigma_u}^C \cdot A^C\right)}{\left(\sigma_u \cdot A\right)} \\ &= \left(1 - 0.19\eta - 0.09\eta^2 - 1.0\eta^3\right) \cdot (1 - \eta).\end{aligned} \tag{13}$$

A practical way to quantify the general corrosion is to use a power law to model the loss of thickness with the service

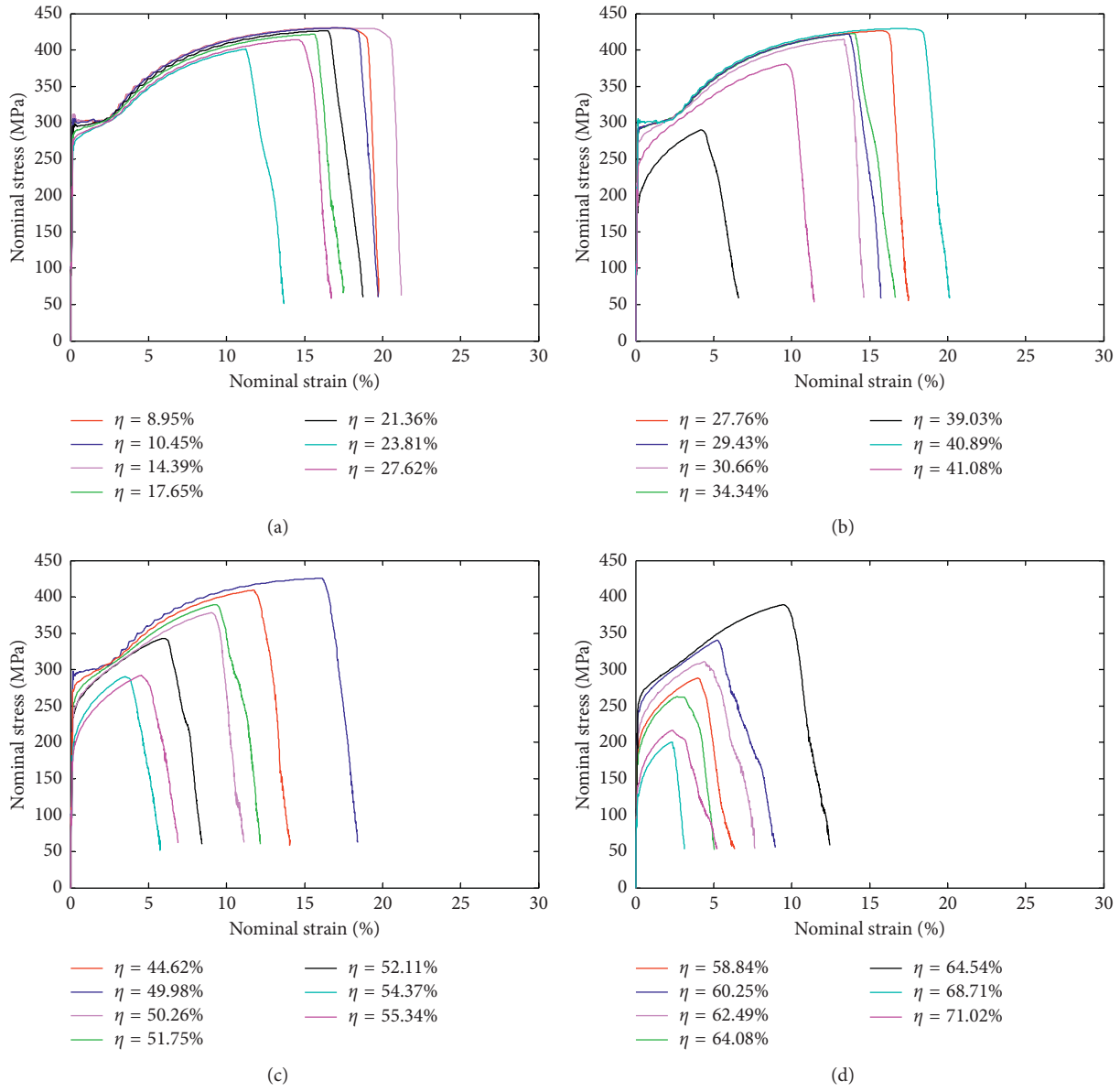

Figure 12: Calculating the nominal stress-strain curve for corroded specimens using equation (10).

time. According to [36], the general form of the corrosion power law can be expressed as

$$\eta = \alpha n_y^{\beta}, \tag{14}$$

in which n_y is the service time in unit year and α, β are corrosion constants. When the pipe is exposed to atmosphere, the values of α, β are suggested to be 0.066, 0.53, which are evaluated for fitting equation (14) to corrosion data [37]. However, when the pipe is immersed in seawater, the values of 0.0833 and 0.8675 are suggested to set to parameters α and β according to the demonstration by Khedmati et al. [38]. Since the marine environment is worse, the service time (n_y) is limited to 16 years.

As shown in Figure 14, the tensile capacity of the corroded pipeline during their service time can be constructed via equations (13) and (14). Clearly, the tensile load capacity of the pipe is sensitive to the service environment and decreases steadily with the service life. When the pipe is exposed to atmosphere during its life, its tensile capacity will be 60% and 35% of the initial state in the 20th and 50th years. However, when the unpainted pipe works in the seawater, its tensile capacity will be 50% of the original state in the 6th year and will be completely lost when it reaches 16 years.

Presently, the stress-based limit analysis is a primary tool to assess the pipeline's integrity and safety. Therefore, equation (12) can be adopted together with the formula suggested by ASME B31G [11] or DNV RP-F101 [13] to predict the mechanical behavior or residual life of the corroded pipeline. At the same time, an energy-based criterion [39–42] appears to provide novel insight into this field and deserves further attention in future work.

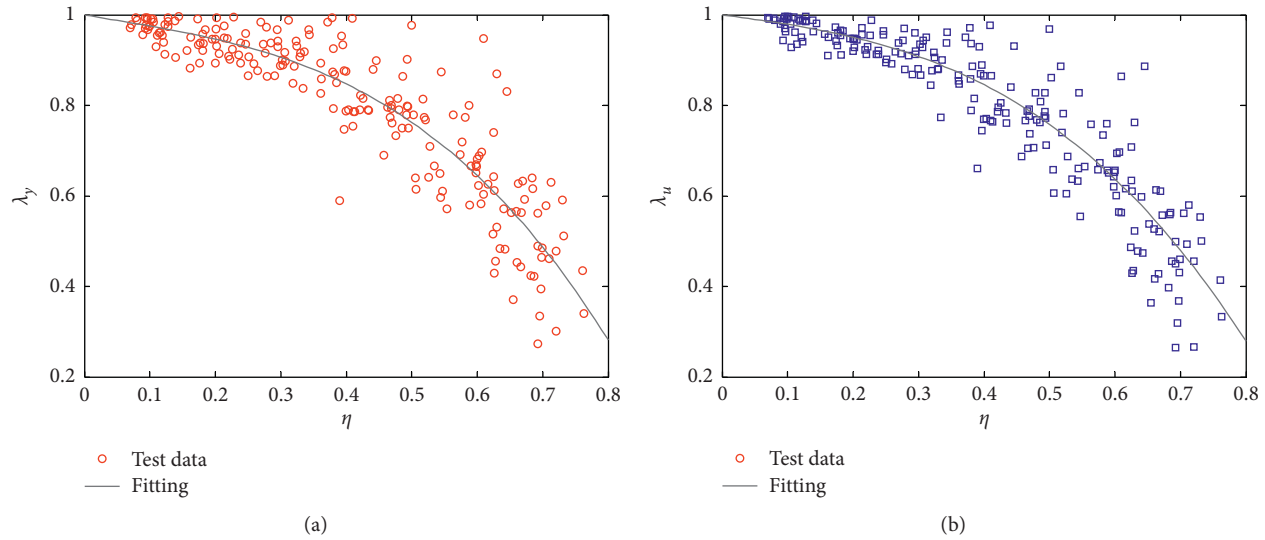

Figure 13: The degrading trend of mechanical properties with the increase of corrosion rate: (a) yield stress; (b) ultimate stress.

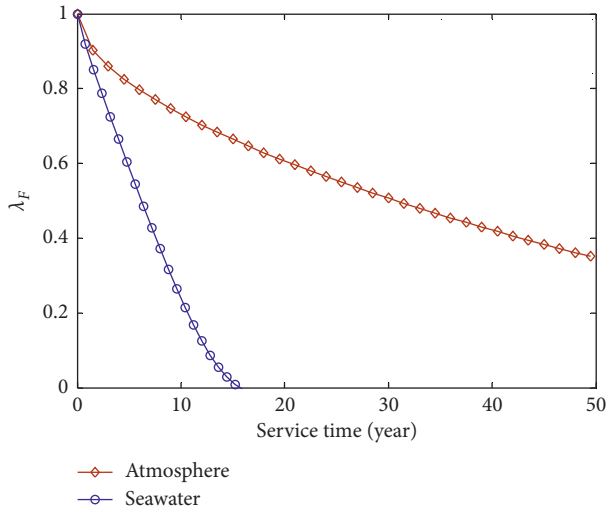

Figure 14: The degradation of tensile capacity with an increase of pipe service time.

6. Conclusion

In this paper, the electrochemical accelerated corrosion method was applied, and 210 standard round steel pipes were corroded from grades of 10% to 70%. The damage characteristics and performance indexes of the pipeline were recorded, characterized, and compared by standard tensile test. Based on this, the influence of corrosion on the tensile fracture of the pipeline was identified. The main conclusions are summarized as follows:

(1) The wall thickness of the pipe will decrease with the environmental erosion, and the nonuniformity will be gradually expanded with the increase of the corrosion rate.

(2) Corroded pipes tend to generate stress concentration at weak locations under axial stretching, so the site of the initial cracks and subsequent expansion paths shows strong randomness. Affected by this, the fractures are mostly characterized by a brittle failure mode lacking the yield plateau and plastic necking.

(3) Under the action of tension, the macroscopic strength index (yield strength, ultimate strength) of the corroded pipeline will show a statistically significant decreasing trend with the increase of the corrosion rate. However, no substantial change in the elastic modulus was observed compared to the uncorroded pipe.

(4) The axial tensile strength of the in-service pipeline is strongly dependent on the corrosion caused by the environmental intrusion, and the reduction of the wall thickness of the pipe and the nonuniformity of the wall thickness variation are the fundamental causes of this dependence.

The data obtained herein provides a quantitative understanding and benchmark for the tensile behavior of the corroded pipeline. The detailed tensile fracture behavior and mechanism for performance degradation are discussed by Liu et al. [43] using numerical simulation. Random distribution fields of the outer wall thickness are constructed to match real section characteristics, and a series of Monte Carlo method-based simulations are carried out there to outline the effects of corrosion rate and thickness variance on the overall response.

Data Availability

The data used to support the findings of this study are included within the article.

Conflicts of Interest

The authors declare that they have no conflicts of interest.

Acknowledgments

This work was supported by the National Science Foundation of China (Grant Nos. 11672165 and 51208289).

References

[1] M. Chen and Y. Jiang, "Effects of prestrain on the tensional function of X60 pipeline steel," *Procedia Engineering*, vol. 26, pp. 1720–1725, 2011.

[2] S. Wu, J. Ren, X. Zhou, G. Cao, Z. Liu, and J. Yang, "Comparisons of different data-driven modeling techniques for predicting tensile strength of X70 pipeline steels," *Transactions of the Indian Institute of Metals*, vol. 72, no. 5, pp. 1277–1288, 2019.

[3] R. H. Talemi, S. Brown, S. Martynov, and H. Mahgerefteh, "Hybrid fluid-structure interaction modelling of dynamic brittle fracture in steel pipelines transporting CO_2 streams," *International Journal of Greenhouse Gas Control*, vol. 54, pp. 702–715, 2016.

[4] V. V. Aleshin and K. Van Den Abeele, "Preisach description for solids with frictional cracks," *International Journal of Nonlinear Mechanics*, vol. 104, pp. 28–38, 2018.

[5] C. I. Ossai, "Advances in asset management techniques: an overview of corrosion mechanisms and mitigation strategies for oil and gas pipelines," *ISRN Corrosion*, vol. 2012, Article ID 570143, 8 pages, 2012.

[6] A. K. Pilkey, S. B. Lambert, and A. Plumtree, "Stress corrosion cracking of X-60 line pipe steel in a carbonate-bicarbonate solution," *Corrosion*, vol. 51, no. 2, pp. 91–96, 1995.

[7] G. Fekete and L. Varga, "The effect of the width to length ratios of corrosion defects on the burst pressures of transmission pipelines," *Engineering Failure Analysis*, vol. 21, pp. 21–30, 2012.

[8] D. Li, C. Xiong, T. Huang, R. Wei, N. Han, and F. Xing, "A simplified constitutive model for corroded steel bars," *Construction and Building Materials*, vol. 186, pp. 11–19, 2018.

[9] A. A. Almusallam, "Effect of degree of corrosion on the properties of reinforcing steel bars," *Construction and Building Materials*, vol. 15, no. 8, pp. 361–368, 2001.

[10] S. Imperatore, Z. Rinaldi, and C. Drago, "Degradation relationships for the mechanical properties of corroded steel rebars," *Construction and Building Materials*, vol. 148, pp. 219–230, 2017.

[11] ASME, *Manual of Determining the Remaining Strength of Corroded Pipelines. A Supplement ANSI/ASME B31G Code for Press Piping*, ASME, New York, NY, USA, 1991.

[12] J. F. Kiefner and P. H. Vieth, *A Modified Criterion for Evaluating the Remaining Strength of Corroded Pipe*, American Gas Association, Washington, DC, USA, 1989.

[13] DNV, *Recommend Practice, RP-F101, Corroded Pipelines*, Det Norske Veritas, Oslo, Norway, 2000.

[14] Y. Bai and S. Hauch, "Collapse capacity of corroded pipes under combined pressure, longitudinal force and bending," *International Journal of Offshore and Polar Engineering*, vol. 11, no. 1, pp. 55–63, 2001.

[15] L.-h. Han, S.-y. He, Y.-p. Wang, and C.-d. Liu, "Limit moment of local wall thinning in pipe under bending," *International Journal of Pressure Vessels and Piping*, vol. 76, no. 8, pp. 539–542, 1999.

[16] Y.-J. Kim, C.-K. Oh, C.-Y. Park, and K. Hasegawa, "Net-section limit load approach for failure strength estimates of pipes with local wall thinning," *International Journal of Pressure Vessels and Piping*, vol. 83, no. 7, pp. 546–555, 2006.

[17] S. H. Kim, Y. S. So, and J. G. Kim, "Fracture behavior of locally corroded steel pipeline in district heating system using the combination of electrochemistry and fracture mechanics," *Metals and Materials International*, pp. 1–8, Springer, Berlin, Germany, 2019.

[18] M. Mokhtari and R. E. Melchers, "A new approach to assess the remaining strength of corroded steel pipes," *Engineering Failure Analysis*, vol. 93, pp. 144–156, 2018.

[19] H. Ye, S. T. Yan, and Z. J. Jin, "Collapse of corroded pipelines under combined tension and external pressure," *PLoS One*, vol. 11, no. 4, Article ID e0154314, 2016.

[20] X.-K. Zhu and B. N. Leis, "Influence of yield-to-tensile strength ratio on failure assessment of corroded pipelines," *Journal of Pressure Vessel Technology*, vol. 127, no. 4, pp. 436–442, 2005.

[21] A. Rajabipour and R. E. Melchers, "A numerical study of damage caused by combined pitting corrosion and axial stress in steel pipes," *Corrosion Science*, vol. 76, pp. 292–301, 2013.

[22] V. I. Kucheryavyi and S. N. Mil'kov, "Evaluation of strength reliability of an oil-and-gas pipeline wall," *Journal of Machinery Manufacture and Reliability*, vol. 46, no. 3, pp. 309–312, 2017.

[23] Z. Kou, "Diameter selection of oil-gas transportation pipelines," *Petroleum Planning & Engineering*, vol. 16, no. 3, pp. 16–18, 2005, in Chinese.

[24] GB/T 228, Metallic materials-tensile testing-part 1: method of test at room temperature, in Chinese.

[25] Y. Wang, J. A. Wharton, and R. A. Shenoi, "Ultimate strength analysis of aged steel-plated structures exposed to marine corrosion damage: a review," *Corrosion Science*, vol. 86, pp. 42–60, 2014.

[26] Z. Wang, B. Liu, Y. Yang et al., "Experimental and numerical studies on corrosion failure of a three-limb pipe in natural gas field," *Engineering Failure Analysis*, vol. 62, pp. 21–38, 2016.

[27] C. Q. Li, "Initiation of chloride-induced reinforcement corrosion in concrete structural members—experimentation," *ACI Structural Journal*, vol. 98, no. 4, pp. 502–510, 2001.

[28] Y. G. Du, L. A. Clark, and A. H. C. Chan, "Residual capacity of corroded reinforcing bars," *Magazine of Concrete Research*, vol. 57, no. 3, pp. 135–147, 2005.

[29] J. L. C. Diniz, R. D. Vieira, J. T. Castro, A. C. Benjamin, and J. L. F. Freire, "Stress and strain analysis of pipelines with localized metal loss," *Experimental Mechanics*, vol. 46, no. 6, pp. 765–775, 2006.

[30] G.-c. Qin, S.-h. Xu, D.-q. Yao, and Z.-x. Zhang, "Study on the degradation of mechanical properties of corroded steel plates based on surface topography," *Journal of Constructional Steel Research*, vol. 125, pp. 205–217, 2016.

[31] T. A. El Maaddawy and K. A. Soudki, "Effectiveness of impressed current technique to simulate corrosion of steel reinforcement in concrete," *Journal of Materials in Civil Engineering*, vol. 15, no. 1, pp. 41–47, 2003.

[32] M. Maslehuddin, I. A. Allam, and G. J. Al-Sulainmani, "Effect of rusting of reinforcing steel on its mechanical properties and bond with concrete," *Materials Journal*, vol. 87, no. 5, pp. 496–502, 1990.

[33] Y.-C. Ou, Y. T. T. Susanto, and H. Roh, "Tensile behavior of naturally and artificially corroded steel bars," *Construction and Building Materials*, vol. 103, pp. 93–104, 2016.

[34] X. Gu, H. Guo, B. Zhou, W. Zhang, and C. Jiang, "Corrosion non-uniformity of steel bars and reliability of corroded RC beams," *Engineering Structures*, vol. 167, pp. 188–202, 2018.

[35] Y. Wang, S. Xu, H. Wang, and A. Li, "Predicting the residual strength and deformability of corroded steel plate based on the corrosion morphology," *Construction and Building Materials*, vol. 152, pp. 777–793, 2017.

[36] A. Amirat, A. Mohamed-Chateauneuf, and K. Chaoui, "Reliability assessment of underground pipelines under the combined effect of active corrosion and residual stress,"

International Journal of Pressure Vessels and Piping, vol. 83, no. 2, pp. 107–117, 2006.

[37] V. Kucera and E. Mattsson, "Atmospheric corrosion," in *Corrosion Mechanics*, F. Mansfeld, Ed., Marcel Dekker, New York, NY, USA, 1987.

[38] M. R. Khedmati, M. M. Roshanali, and Z. H. M. E. Nouri, "Strength of steel plates with both-sides randomly distributed with corrosion wastage under uniaxial compression," *Thin-Walled Structures*, vol. 49, no. 2, pp. 325–342, 2011.

[39] P. Gallo, Y. Hagiwaraa, T. Shimada et al., "Strain energy density approach for brittle fracture from nano to macroscale and breakdown of continuum theory," *Theoretical and Applied Fracture Mechanics*, vol. 103, pp. 1–7, 2019.

[40] P. Gallo, T. Sumigawa, T. Kitamura, and F. Berto, "Evaluation of the strain energy density control volume for a nanoscale singular stress field," *Fatigue & Fracture of Engineering Materials & Structures*, vol. 39, no. 12, pp. 1557–1564, 2016.

[41] P. Gallo, T. Sumigawa, T. Kitamura, and F. Berto, "Static assessment of nanoscale notched silicon beams using the averaged strain energy density method," *Theoretical and Applied Fracture Mechanics*, vol. 95, pp. 261–269, 2018.

[42] F. Berto and P. Gallo, "Extension of linear elastic strain energy density approach to high temperature fatigue and a synthesis of Cu-Be alloy experimental tests," *Engineering Solid Mechanics*, vol. 3, no. 2, pp. 111–116, 2015.

[43] F. Liu, Y. C. Yang, and F. Xi, "Tensile fracture behavior of corroded pipeline, part 2: numerical simulation based on Monte carlo method," *Advances in Materials Science & Engineering*, under review.